

# Hybrid version of the tilted axis cranking model and its application to $^{128}\text{Ba}$

V. I. Dimitrov, F. Dönau, and S. Frauendorf

*Institut für Kern- und Hadronenphysik, Forschungszentrum Rossendorf, PB 51 01 19, D-01314 Dresden, Germany  
and Department of Physics, University of Notre Dame, Notre Dame, Indiana 46556*

(Received 16 February 2000; published 20 July 2000)

A hybrid version the deformed nuclear potential is suggested, which combines a spherical Woods-Saxon potential with a deformed Nilsson potential. It removes the problems of the conventional Nilsson potential in the mass 130 region. Based on the hybrid potential, tilted axis cranking calculations are carried out for the magnetic dipole band in  $^{128}\text{Ba}$ .

PACS number(s): 21.10.-k, 25.70.Gh, 27.60.+j

## I. INTRODUCTION

The transitional nuclei in the region  $A = 130-140$  show regular  $\Delta I = 1$  bands, characterized by large  $B(M1)/B(E2)$  ratios, a lack of signature splitting and relatively low dynamical moments of inertia [1]. These bands have an intermediate character. They stand between the collective high- $K$  bands of well-deformed nuclei, for which collective rotation is the dominant mechanism of generating the angular momentum, and the magnetic rotation of near spherical nuclei, for which few high- $j$  particles and holes generate most of the angular momentum by means of the shears mechanism (see, for example [2,3]). The question of how magnetic rotation changes into collective one has not been studied yet. So far, only the magnetic dipole band in  $^{128}\text{Ba}$  has been investigated [4] from this point of view. Another intriguing question is the possibility of a chiral character of rotation [5]. Their softness with respect to triaxial deformations makes the nuclei in the  $A = 130$  region particularly good candidates for identifying this new symmetry type.

The tilted axis cranking (TAC) model [6] has turned out to be an appropriate theoretical tool for the description of the magnetic dipole bands. This model is a natural generalization of the cranking model [7] for situations where the axis of rotation does not coincide with a principal axis of the density distribution of the rotating nucleus, and thus the signature is not a good quantum number. Since introduced, TAC has proven to be a reliable approximation for the energies and intraband transitions in both normally and weakly deformed nuclei [3]. However, in the case of the four quasiparticle magnetic dipole band in  $^{128}\text{Ba}$ , the TAC calculations [4] predicted the wrong parity and a too early termination of the band [8-10].

$^{128}\text{Ba}$  is one of the best studied nuclei in this mass range and the above mentioned  $\Delta I = 1$  rotational band is a good test case for the TAC model. The purpose of the present work is to identify the origin of the discrepancies and remove them. The version of TAC used in [4] was based on the Nilsson Hamiltonian with the standard set of parameters [11]. This parameter set is known to have problems in the  $A = 130$  region [12,13] and a better set has been suggested in Ref. [13]. We attribute the discrepancies of the TAC calculations for  $^{128}\text{Ba}$  [4] with the later measurements [8-10] to the general problems of the standard parameter set for the Nilsson potential in this region. We shall repeat the TAC

calculations for optimized parameter set of Ref. [13].

The Woods-Saxon potential with the universal parameter set [14] works very well around  $A = 130$  [15]. Moreover, it is expected that this potential, which has a realistic radial profile instead of the artificial  $l^2$  term of the Nilsson model, is more reliable when exploring mass regions where the Nilsson parameters have not been locally optimized. Moreover, the  $l^2$  dependence of the Nilsson potential is known to be problematic when the mean field is cranked at high angular velocity. A TAC version based on the Woods-Saxon potential has been developed but not yet fully tested. In this paper we use an approximation which we call the hybrid potential. It consists in adapting the Nilsson potential as close as possible to the Woods-Saxon one. Instead of the parametrizing the single particle levels of the spherical modified oscillator in the standard way by means of an  $ls$  and an  $l^2$  term, the hybrid model directly takes the energies of the spherical Woods-Saxon potential. The deformed part of the hybrid potential is an anisotropic harmonic oscillator. This compromise keeps the simplicity of the Nilsson potential, because coupling between the oscillator shells can be approximately taken into account by means of stretched coordinates [11], and it amounts to a minor modification of the existing TAC code. On the other hand, it has turned out to be quite a good approximation of the realistic flat bottom potential as long as the deformation is moderate. The hybrid potential was used to calculate the triaxial shapes of liquid sodium clusters [16]. The results agree very well with later calculations using the correct radial profile of the deformed part of the potential [17]. Another motivation for the hybrid potential is the considerably lower computation time (about a factor of 10) as compared with the full Woods-Saxon potential, which is important for the TAC calculations, which demand to achieve self-consistency in two extra dimensions (the orientation angles).

## II. TAC IMPLEMENTATION

The TAC model is discussed in more detail in [2,3,6,18]. The brief presentation in this paper focuses at the suggested improvement of this approach. The starting point is the mean field Routhian<sup>1</sup>

<sup>1</sup>For simplicity, only one type of particle is spelled out. The extension to both types is obvious.

$$h' = h_{\text{sph}} + V_{\text{def}}(\varepsilon_2, \gamma, \varepsilon_4) - \Delta(P + P^+) - \lambda N - \omega(\sin \vartheta j_1 + \cos \vartheta j_3), \quad (1)$$

where  $h_{\text{sph}}$  denotes the spherical part including the spin-orbit term and  $V_{\text{def}}(\varepsilon_2, \gamma, \varepsilon_4)$  the deformed part of the Nilsson single-particle Hamiltonian (see, e.g., [11]). The pairing field in Eq. (1) is determined by the gap parameter  $\Delta$  and the monopole pairing operator  $P = \sum_k c_k c_{\bar{k}}$  while the chemical potential  $\lambda N$  is needed to satisfy on average the particle number conservation. The two-dimensional cranking term  $\omega(\sin \vartheta j_1 + \cos \vartheta j_3)$  is the new element of the TAC, as compared to the standard cranking model, which is recovered for  $\vartheta = 0$  or  $90^\circ$ . The angle  $\vartheta$  fixes the tilt of the cranking axis with respect to the intrinsic three-axis within the principal (1–3) plane of the deformed potential. By diagonalization in stretched coordinates, neglecting  $\Delta N = 2$  shell mixing, this TAC Routhian yields quasiparticle energies and quasiparticle states, from which the many-body configuration  $|\omega, \varepsilon_2, \gamma, \varepsilon_4, \vartheta\rangle$  of interest is constructed.

The mean field is found for a given frequency  $\omega$  and fixed configuration by minimizing the total Routhian

$$E'(\omega, \varepsilon_2, \gamma, \varepsilon_4, \vartheta) = \langle \omega, \varepsilon_2, \gamma, \varepsilon_4, \vartheta | h' | \omega, \varepsilon_2, \gamma, \varepsilon_4, \vartheta \rangle \quad (2)$$

with respect to the deformation parameters  $(\varepsilon_2, \gamma, \varepsilon_4)$  and the tilt angle  $\vartheta$ . The value of  $\Delta$  is kept fixed at two values: 80% of the experimental odd-even mass difference and zero. At the equilibrium angle  $\vartheta = \vartheta_0$  (minimum) the cranking axis is parallel to the direction of the angular momentum vector  $\vec{J} = (\langle j_1 \rangle, \langle j_3 \rangle)$ . After the minimum is found the various electromagnetic observables of interest are obtained by means of the following semiclassical expressions [2,18]:

$$\begin{aligned} & \langle I-2I-2 | \mathcal{M}_{-2}(E2) | II \rangle \\ &= \langle \mathcal{M}_{-2}(E2) \rangle \\ &= \sqrt{\frac{5}{4\pi}} \left( \frac{eZ}{A} \right) \left[ \sqrt{\frac{3}{8}} \langle Q'_0 \rangle (\sin \vartheta)^2 \right. \\ & \quad \left. + \frac{1}{4} \langle Q'_2 + Q'_{-2} \rangle (1 + (\cos \vartheta)^2) \right], \\ & \langle I-1I-1 | \mathcal{M}_{-1}(E2) | II \rangle \\ &= \langle \mathcal{M}_{-1}(E2) \rangle \\ &= \sqrt{\frac{5}{4\pi}} \left( \frac{eZ}{A} \right) \left[ \sin \vartheta \cos \vartheta \right. \\ & \quad \left. \times \left( \sqrt{\frac{3}{2}} \langle Q'_0 \rangle - \frac{1}{2} \langle Q'_2 + Q'_{-2} \rangle \right) \right] \quad (3) \\ & \langle I-1I-1 | \mathcal{M}_{-1}(M1) | II \rangle \\ &= \langle \mathcal{M}_{-1}(M1) \rangle \\ &= \sqrt{\frac{3}{8\pi}} [\langle \mu_3 \rangle \sin \vartheta - \langle \mu_1 \rangle \cos \vartheta], \end{aligned}$$

where  $\langle \mathcal{M}_\nu \rangle$  is the expectation value of the transition operator with the TAC configuration  $|\rangle$ , the components of which refer to the laboratory system. The intrinsic quadrupole moments  $Q'_\mu$  are calculated with respect to the principle axes (1, 2, 3). The same holds for the magnetic moments

$$\mu_i = \mu_N (J_{i,p} + (\eta 5.58 - 1) S_{i,p} - \eta 3.82 S_{i,n}), \quad (4)$$

where the free nucleonic magnetic moments are attenuated by a factor of  $\eta = 0.7$ . The reduced transition probabilities are

$$B(M1, \Delta I = 1) = \langle \mathcal{M}_{-1}(M1) \rangle^2,$$

$$B(E2, \Delta I = 2) = \langle \mathcal{M}_{-2}(E2) \rangle^2.$$

The mixing ratio is

$$\delta = \frac{\langle \mathcal{M}_{-1}(E2) \rangle}{\langle \mathcal{M}_{-1}(M1) \rangle}. \quad (5)$$

We apply the Strutinsky renormalization procedure to calculate the total Routhian

$$E'(\omega) = E_{\text{LD}}(\omega = 0) - E_{\text{smooth}} + \langle \omega | h' | \omega \rangle, \quad (6)$$

where  $E_{\text{LD}} = E_{\text{LD}}(\varepsilon_2, \gamma, \varepsilon_4, \varepsilon_4)$  means the liquid drop energy and  $E_{\text{smooth}}$  is the smooth part of the mean-field energy calculated from the single-particle energies at  $\omega = 0$ . This version of the TAC has turned out to be quite successful for well-deformed nuclei (see [2,3,18] and references therein).

The new element of the present paper consists in the hybrid potential, which approximates the well-established deformed Woods-Saxon potential, yet preserving the existing convenient TAC environment. For this purpose the spherical part  $h_{\text{sph}}$  in Eq. (1) is replaced the spherical Woods-Saxon Hamiltonian for the nucleus of interest. In the present work the universal Woods-Saxon parameters are used (see, e.g., [14]).

Technically, the replacement is rather simple, because the existing TAC code uses states of good  $l, j, m$  as a basis. The spherical Nilsson energies  $e_{N,l,j}^{(\text{nil})}$  are replaced by the spherical Woods-Saxon energies  $e_{N,l,j}^{(\text{ws})}$ . It turns out to be unproblematic to associate the quantum numbers of the two different potentials. For a given combination  $l, j$  the third quantum number  $N$  is found by counting from the state with the lowest energy. The fact that the spherical Woods-Saxon code uses a harmonic oscillator basis permitted a check of the algorithm. The major component of the Woods-Saxon wave function agrees with the state found by our counting algorithm. In the high-lying part of the single-particle spectrum (three shells above the valence shell or higher) there are occasional ambiguities in assigning the states. Small errors of this kind are not expected to have any consequences at mod-

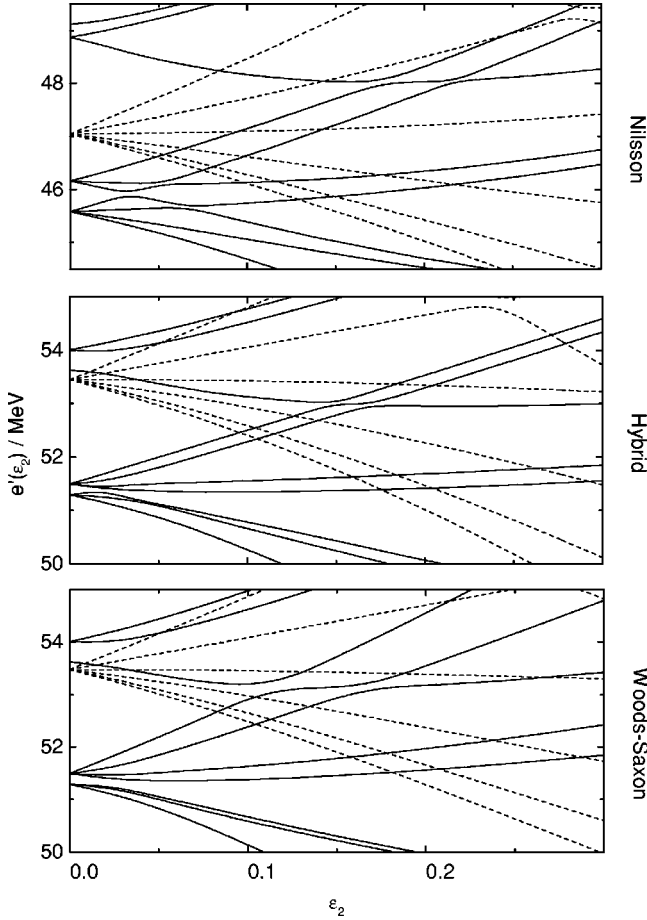


FIG. 1. Proton single-particle levels as a function of deformation for the Woods-Saxon (bottom), hybrid (middle), and Nilsson (top) models, respectively. Full lines present positive parity states, broken lines present negative parity states. The Fermi energy lies at about 51.3 MeV for the Woods-Saxon and the hybrid models and at 45.6 MeV for the Nilsson model.

erate or small deformation. The states do not couple strongly to the states near the Fermi surface. They contribute only to the smooth level density used in the Strutinsky renormalization, which will not be affected by small shifts of the levels.

Such a replacement of the spherical single-particle energies is a common practice in large scale shell-model configuration mixing and similar calculations, where they are often used as adjustable parameters [19]. The effect of the replacement is illustrated on Fig. 1, which shows the deformation dependence of the proton single-particle levels of  $^{128}\text{Ba}$  for the Nilsson Hamiltonian with the standard and optimized parameters, the Woods-Saxon and the hybrid Hamiltonians. The close similarity of the levels of the Woods-Saxon and the hybrid models is obvious. The hybrid has a somewhat later and sharper crossing between the positive parity levels, which also show stronger tendency to arrange into pairs of pseudo spin doublets. These traits are inherited from the Nilsson Hamiltonian, which controls the change with deformation. The main difference between the Nilsson Hamiltonian with standard parameters and the other is the lower energy of the negative parity levels originating from  $h_{11/2}$ . It seems to be the reason for the discrepancies between the

previous TAC predictions and the experiment, as will be demonstrated in the next section. Reference [13] demonstrated that the optimized Nilsson levels and the Woods-Saxon levels are very similar. The hybrid levels agree with the optimized Nilsson levels with the same accuracy. Hence one expects similar TAC results for the two models.

### III. THE M1 BAND IN $^{128}\text{Ba}$

In the previous TAC calculations for the  $\Delta I=1$  band in  $^{128}\text{Ba}$  [4] the four quasiparticle configurations<sup>2</sup>  $[\pi(h_{11/2})^2\nu(h_{11/2}(d_{5/2}g_{7/2}))]$  for the negative parity and  $[\pi(h_{11/2})^2\nu(h_{11/2})^2]$  for the positive parity were found to be the lowest ones in energy at the oblate deformation of  $\epsilon = 0.26$ ,  $\gamma = 60^\circ$ . This deformation was determined at  $\omega = 0.2$  MeV by minimizing the total Routhian calculated from the quadrupole-quadrupole interaction. With the present version of TAC we find a significantly smaller prolate equilibrium deformation of  $\epsilon = 0.205$  and  $\gamma = 0^\circ$ . The lowest four quasiparticle configuration now turns out to be  $[\pi(h_{11/2}(d_{5/2}g_{7/2}))\nu(h_{11/2}(d_{5/2}g_{7/2}))]$ . Figure 2 shows the quasiproton and quasineutron levels for various cranking frequencies at tilt angle  $\vartheta = 90^\circ$  and for various angles at  $\omega = 0.2$  MeV. The equilibrium value of  $\vartheta$ , which minimizes  $E'$ , is found to be  $\vartheta_0 = 52.5^\circ$  for  $\omega = 0.2$  MeV.

As seen, the different position of the  $h_{11/2}$  orbitals in the hybrid TAC has drastic consequences. The deformation changes from oblate to prolate, resulting in a different configuration of the M1 band. This is not surprising in a region where the energy difference between oblate and prolate shape is small.

The calculations of the  $\Delta I=1$  band in the present work are built on this new configuration

$$[\pi(h_{11/2}(d_{5/2}g_{7/2}))\nu(h_{11/2}(d_{5/2}g_{7/2}))],$$

which is the lowest four-quasiparticle TAC solution. In agreement with the experiment, it has positive parity. The excitation of four quasiparticles significantly reduces the pairing gaps. In order to better grasp the influence of this blocking on characteristics of the band, we did two calculations: one with  $\Delta_\nu = 0.88$  MeV and  $\Delta_\pi = 1.04$  MeV corresponding to 80% of the experimental even odd mass difference and one with zero pairing.

Electromagnetic transition properties present a stringent test of the nuclear models. The experimental information about lifetimes and mixing ratios of the magnetic dipole band was accumulated in several experiments [8–10]. Figure 3 compares the experimental  $B(M1)$  and  $B(E2)$  values and mixing ratios with the results of TAC model obtained for the configuration  $[\pi(h_{11/2}(d_{5/2}g_{7/2}))\nu(h_{11/2}(d_{5/2}g_{7/2}))]$ . All electromagnetic characteristics of the band are well reproduced by both the paired and unpaired calculations. Curiously, the quenching of pairing influences to some extent the  $B(M1)$

<sup>2</sup>Indicating the major components, we denote the mixed Nilsson state by  $(d_{5/2}g_{7/2})$ .

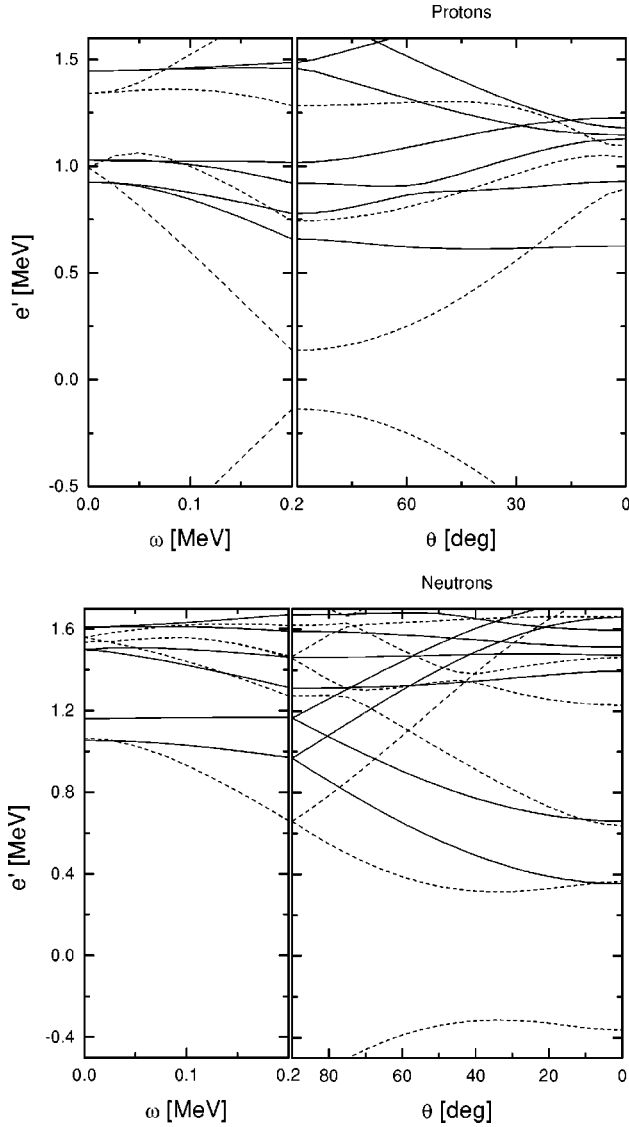


FIG. 2. Proton (a) and neutron (b) quasiparticle levels as a function of rotational frequency  $\hbar\omega$  and tilt angle  $\vartheta$ . Full lines correspond to positive parity, broken lines correspond to negative parity states. In both cases the lowest two quasiparticle configurations involve one predominantly  $(d_{5/2}g_{7/2})$  and one predominantly  $h_{11/2}$  state. The deformation parameters are  $\varepsilon_2=0.205, \varepsilon_4=-0.01, \gamma=0^\circ$ , which are the equilibrium values at  $\omega=0.2$  MeV.

values but leaves almost unchanged the  $B(E2)$  values up to spin  $18\hbar$ . The TAC calculation seems to slightly overestimate the deformation.

In contrast with the previous TAC calculation, it is possible to follow the band all the way up to spin  $26\hbar$ . Figure 4 shows the measured and the calculated function  $J(\omega)$  of the spin on the angular frequency. It is more sensitive to the changes of the pair correlations. While the unpaired calculation gives a nearly linear function with the moment of inertia  $\mathcal{J}^{(2)}=dJ/d\omega$  close to the measured one, the paired calculation exhibits a substantially lower moment of inertia for low rotational frequencies and an upbend at higher ones. The experiment is in between. This seems to indicate that the pair field is weak in this nucleus and a more refined treatment of

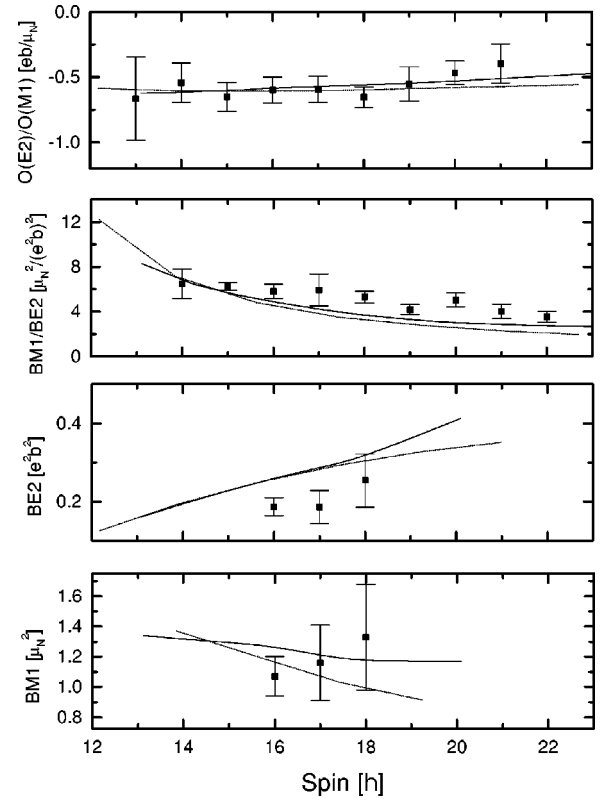


FIG. 3. Electromagnetic observables as obtained by paired calculation (full lines), unpaired calculation (dotted lines), and experiment.

pairing is needed. It is noted that in the calculations the band extends down to  $\omega=0.1$  MeV and  $J=11\hbar$ . In experiment there is an irregularity around  $I=12,13\hbar$ . It may be caused by mixing of the  $13^+$  state with another  $13^+$  state, which lies nearby in energy ( $\Delta E=0.045$  MeV) and into which the  $14^+$  also decays [10].

In [8–10], the  $\Delta I=1$  band was analyzed in terms of a pure high- $K$  band using the familiar expressions for the  $B(M1)$  and  $B(E2)$  values for the axial symmetric rotor [20]. Adjusting three free parameters, the  $K$  value, the intrinsic quadrupole moment  $Q_0$ , and the gyromagnetic factor  $|g_K - g_R|$ , a good fit of the electromagnetic decay data was obtained. The quality is practically the same as in our calculation without parameters in Fig. 4. The TAC calculation contains much more physical information as, e.g., the specific configuration on which the band is built and the band energies. The knowledge of the intrinsic state can be used to derive further structure information, e.g., the geometrical coupling scheme shown in Fig. 5, which enables one to see how the total spin is formed from the quasiparticle orbitals and how it changes with the rotational frequency. Apparently, most of the angular momentum gain along the band is of collective nature, however the high- $j$  quasiparticles from proton and neutron ( $d_{5/2}g_{7/2}$ ) and  $h_{11/2}$  orbitals do also substantially contribute by means of the shears mechanism. With increasing frequency, the three-component of the spin vector  $\vec{J}$  stays practically at  $\langle J_3 \rangle \approx 9\hbar$ . However, this does not mean that the corresponding TAC configuration behaves

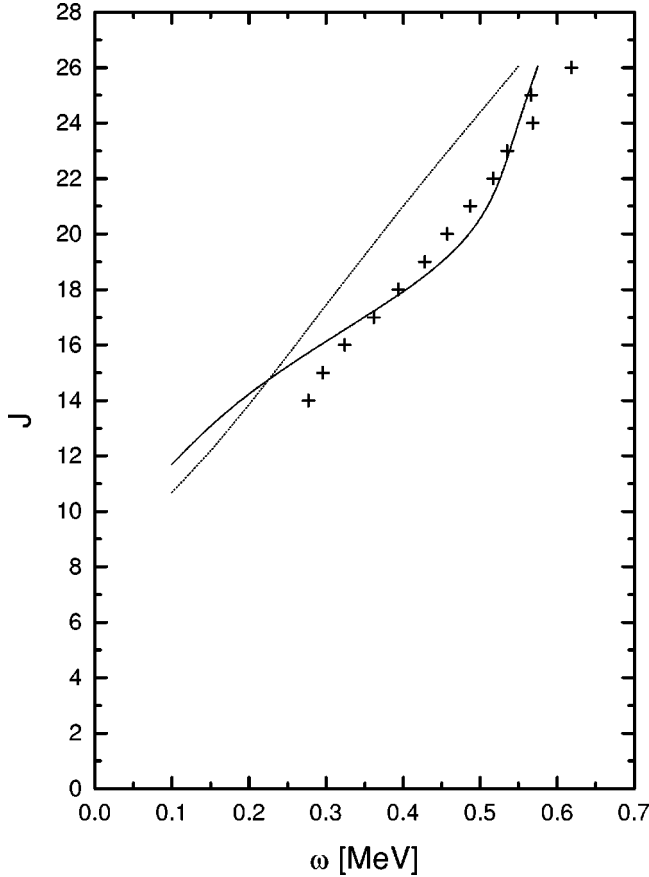


FIG. 4. Dependence of the angular momentum  $J=I$  on the rotational frequency  $\hbar\omega$  as obtained by paired calculation (full line), unpaired calculation (dotted line), and experiment (crosses). The experimental frequency is extracted from the measured  $\gamma$ -energy data using the relations  $\hbar\omega(I) = E_\gamma = E(I) - E(I-1)$ .

like a structureless high- $K$  rotor. Figure 6 shows that the calculated dependence  $\vartheta(\omega)$  of the tilt angle on the rotational frequency by no means follows curve expected for the strong coupling limit. Thus, the present case lies in between a good shears band and a good high- $K$  band. The  $\Delta I=1$  band in  $^{128}\text{Ba}$  is an example for a rotational band of intermediate nature.

#### IV. COMPARISON WITH THE OPTIMIZED NILSSON POTENTIAL

The similarity of the single particle levels of the nonrotating hybrid and optimized Nilsson potentials suggests that the rotational behavior should not differ much. This is born out by the TAC calculations. The angular momentum and the transition probabilities are compared in Table I for the case of finite pairing. They are very similar. We find a larger deformation of  $\varepsilon_2=0.24$  and  $\gamma=8^\circ$  for the optimized Nilsson potential. The larger deformation causes an increase of the collective moment of inertia but a decrease of the alignment of the four quasiparticles with the rotational axis (shears mechanism). The two effects contribute with opposite sign to the total angular momentum, which remains almost the same. The weaker shears mechanism for the opti-

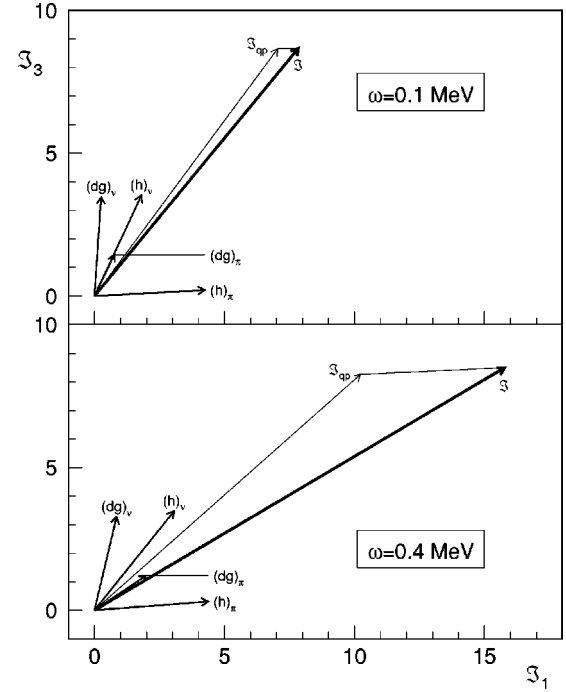


FIG. 5. Spin decomposition in terms of individual quasiparticle contributions for two different rotational frequencies. Quasiparticle configurations are denoted by their predominant components.

mized Nilsson potential leads to the larger  $B(M1)$  values. For the  $B(E2)$  values the effect of the increased deformation is compensated by the somewhat smaller tilt angle  $\vartheta$ .

#### V. SUMMARY

The strength of the TAC model is that it can predict the appearance of  $\Delta I=1$  rotational bands and is able to describe microscopically their electromagnetic decay properties. This is achieved by taking into consideration the orientation of the rotational axis with respect to the deformed potential, which is fixed along a principal axis in the conventional cranking model. The intrinsic TAC configuration of a rotational band

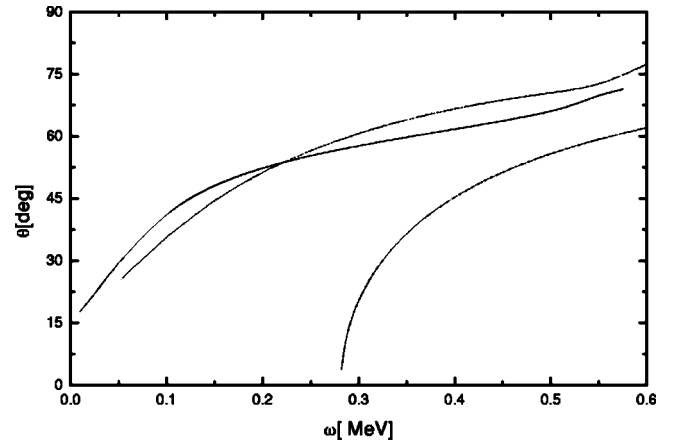


FIG. 6. Equilibrium tilt angle  $\vartheta$  as a function of the rotational frequency  $\hbar\omega$ . Full line, paired calculation; dotted line, unpaired calculation; broken-dotted line, strong coupling limit result.

TABLE I. Tilt angle, spin, and EM observables of the hybrid potential (H) and the optimized Nilsson (ON) models at their corresponding equilibrium deformations for various rotational frequencies.

$\omega$ [MeV]	$\vartheta$ [deg]		$J$ [ $\hbar$ ]		$B(M1)$ [ $\mu_N^2$ ]		$B(E2)$ [ $e^2b^2$ ]	
	H	ON	H	ON	H	ON	H	ON
0.20	52.5	50.7	13.8	13.8	1.31	1.68	0.20	0.20
0.35	55.4	53.3	14.7	14.7	1.29	1.57	0.24	0.23
0.30	57.7	55.4	15.6	15.6	1.26	1.47	0.26	0.26
0.35	59.8	57.4	16.5	16.4	1.21	1.38	0.29	0.29
0.40	61.7	59.3	17.4	17.2	1.17	1.29	0.31	0.32

is found by searching for a local minimum on the multiparameter surface of the total Routhian. Therefore, it is crucial to calculate these surfaces as reliable as possible. In the present work the Strutinsky renormalization and a hybrid single-particle potential were implemented in order to start from a deformed potential, which is reliable in a wide range of  $N$  and  $Z$ . The hybrid potential combines the spherical Woods-Saxon single-particle energies with the deformed part of the Nilsson potential. For moderately deformed nuclei it gives deformed single-particle levels that are quite close to the deformed Woods-Saxon levels.

We applied the hybrid TAC to the previously investigated four quasiparticle magnetic dipole band in  $^{128}\text{Ba}$ . The

lowest equilibrium configuration is found to be  $[\pi(h_{11/2}(d_{5/2}g_{7/2}))\nu(h_{11/2}(d_{5/2}g_{7/2}))]$ . It has positive parity and a prolate axial deformation of  $\epsilon_2=0.20$ . The microscopic TAC calculations describes rather well the experimental energies,  $B(M1)$  and  $B(E2)$  values, as well as the branching and mixing ratios. The dipole band in  $^{128}\text{Ba}$  has an intermediate structure. A comparable amount of angular momentum is generated by the shears mechanism, active for the  $h_{11/2}$  and  $(d_{5/2}g_{7/2})$  quasiparticles, and by collective rotation. It is an example for the transition from collective to magnetic rotation.

The hybrid potential turned out to be crucial for the good agreement between the calculation and the data on  $^{128}\text{Ba}$ . The Nilsson potential with the parameters optimized for the  $A=130$  region gave similar good results. Both potentials seem to be a promising starting point for studying the intriguing interplay between triaxial deformation and the orientation of the rotational axis. The treatment of the pairing needs improvement, because only the cases of a strong and a zero neutron pair field were studied.

#### ACKNOWLEDGMENTS

V.D. wishes to thank the Foundation ‘‘Bulgarian Science and Culture’’ for its support. We thank Professor P. von Brentano and Dr. I. Wiedenhöver, who kept us up with the data. The work was partially carried out under Grant No. DE-FG02-95ER40934.

- 
- [1] See, for example, D. Fossan, J. R. Hughes, Y. Liang, R. Ma, E. S. Paul, and N. Xu, Nucl. Phys. **A520**, 241c (1990).
- [2] S. Frauendorf, Z. Phys. A **385**, 163 (1997).
- [3] S. Frauendorf, Nucl. Phys. A (in press).
- [4] F. Döna, S. Frauendorf, P. von Brentano, A. Gelberg, and O. Vogel, Nucl. Phys. **A584**, 241 (1995).
- [5] S. Frauendorf and J. Meng, Nucl. Phys. **A617**, 131 (1997).
- [6] S. Frauendorf, Nucl. Phys. **A557**, 259c (1993).
- [7] P. Ring and P. Schuck, *The Nuclear Many Body Problem* (Springer, New York, 1980).
- [8] O. Vogel, A. Dewald, P. von Brentano, J. Gableske, R. Krücken, N. Nicolay, A. Gelberg, P. Petkov, A. Gizon, J. Gizon, D. Bazacco, C. Rossi Alvarez, S. Lunardi, P. Pavan, D. R. Napoli, S. Frauendorf, and F. Döna, Phys. Rev. C **56**, 1338 (1997).
- [9] P. Petkov, J. Gableske, O. Vogel, A. Dewald, P. von Brentano, R. Krücken, R. Peusquens, N. Nicolay, A. Gizon, J. Gizon, D. Bazacco, C. Rossi Alvarez, S. Lunardi, P. Pavan, D. R. Napoli, W. Andrejtscheff, and R. V. Jolos, Nucl. Phys. **A640**, 293 (1998).
- [10] I. Wiedenhöver, O. Vogel, H. Klein, A. Dewald, P. von Brentano, J. Gableske, R. Krücken, N. Nicolay, A. Gelberg, P. Petkov, A. Gizon, D. Bazzacco, C. Rossi Alvarez, G. de Angelis, S. Lunardi, P. Pavan, D. R. Napoli, S. Frauendorf, F. Döna, R. V. F. Janssens, and M. Carpender, Phys. Rev. C **58**, 721 (1998).
- [11] S. G. Nilsson and I. Ragnarsson, *Shapes and Shells in Nuclear Structure* (Cambridge University, Cambridge, 1995).
- [12] R. Bengtsson (private communication).
- [13] Jing-ye Zhang, N. Xu, D. B. Fossan, Y. Liang, R. Ma, and E. S. Paul, Phys. Rev. C **39**, 714 (1989); *ibid.* **42**, 1394 (1990).
- [14] S. Cwiok, J. Dudek, W. Nazarewicz, J. Skalski, and T. Werner, Comput. Phys. Commun. **46**, 379 (1987).
- [15] R. Wyss, A. Granderath, R. Bengtsson, P. von Brentano, A. Dewald, A. Gelberg, A. Gizon, J. Gizon, S. Harissopoulos, A. Johnson, W. Lieberz, W. Nazarewicz, J. Nyberg, and K. Schiffer, Nucl. Phys. **A505**, 337 (1989).
- [16] S. Reimann, S. Frauendorf, and M. Brack, Z. Phys. D: At., Mol. Clusters **34**, 125 (1995).
- [17] B. Montag, Th. Hirschmann, J. Meyer, P.-G. Reinhard, and M. Brack, Phys. Rev. B **52**, 4775 (1995).
- [18] S. Frauendorf (unpublished).
- [19] M. Ted Ressel, Maurice B. Aufderheide, Steward D. Bloom, Kim Griest, Grant J. Mathews, and David A. Resler, Phys. Rev. D **48**, 5519 (1993); V. I. Dimitrov, J. Engel, and S. Pittel, *ibid.* **51**, R291 (1995).
- [20] A. Bohr and B. M. Mottelson, *Nuclear Structure*, Vol. II (Benjamin, Reading, MA, 1957).